Aerosol Science and Technology

ISSN: 0278-6826 (Print) 1521-7388 (Online) Journal homepage: http://www.tandfonline.com/loi/uast20

# Dependence of CPC cut-off diameter on particle morphology and other factors

Thomas Tuch, Kay Weinhold, Maik Merkel, Andreas Nowak, Tobias Klein, Paul Quincey, Mark Stolzenburg & Alfred Wiedensohler

**To cite this article:** Thomas Tuch, Kay Weinhold, Maik Merkel, Andreas Nowak, Tobias Klein, Paul Quincey, Mark Stolzenburg & Alfred Wiedensohler (2016) Dependence of CPC cut-off diameter on particle morphology and other factors, Aerosol Science and Technology, 50:4, 331-338, DOI: 10.1080/02786826.2016.1152351

**To link to this article:** http://dx.doi.org/10.1080/02786826.2016.1152351

Accepted author version posted online: 12 Feb 2016.

AEROSOL SCIENCE AND TECHNOLOGY
2016, VOL. 50, NO. 4, 331–338
http://dx.doi.org/10.1080/02786826.2016.1152351



# Dependence of CPC cut-off diameter on particle morphology and other factors

Thomas Tuch[a], Kay Weinhold[a], Maik Merkel[a], Andreas Nowak[b], Tobias Klein[b], Paul Quincey[c], Mark Stolzenburg[d], and Alfred Wiedensohler[a]

[a]Experimental Aerosol and Cloud Microphysics, Leibniz Institute for Tropospheric Research, Leipzig, Germany; [b]Physikalisch-Technische Bundesanstalt, Braunschweig, Germany; [c]Environment Division, National Physical Laboratory, Teddington, United Kingdom; [d]Department of Mechanical Engineering University of Minnesota, Minneapolis, Minnesota, USA

**ABSTRACT**

In this investigation, we summarize performance parameters of 24 TSI CPCs model 3772 and 9 TSI CPCs model 3790 determined at the World Calibration Aerosol Centre Physics hosted by the Leibniz Institute for Tropospheric Research. Model 3790 CPCs are basically identical to model 3772 laminar continuous flow type butanol-based CPCs with a modified temperature difference between saturator and condenser. The average 50% detection efficiency for silver particles for 3772 and 3790 instruments was found to be 7.52 ± 0.04 nm and 24.34 ± 0.29 nm (average mobility diameter ± standard deviation), respectively. Small changes of the temperature difference between saturator and condenser cause larger shifts of the 50% detection efficiencies of 3790 CPCs compared to 3772 CPCs. In addition to the known calibration material dependence of the 50% detection efficiencies of 3790 CPCs, we found a dependence on the morphology of the particles used for calibration. In our experiments more spherical particles shifted the 50% detection efficiencies towards larger mobility diameters.

**ARTICLE HISTORY**
Received 4 August 2015
Accepted 19 January 2016

**EDITOR**
Susanne V. Hering



## Introduction

Condensation particle counters (CPCs) are widely used for environmental research, clean room monitoring and legal compliance measurements in industry. Most of today's CPCs used in state-of-the-art techniques are continuous flow, single-particle-counting instruments as described by Agarwal and Sem (1980) based on the design by Sinclair and Hoopes (1975) and Bricard et al. (1976). Among the first widespread commercial instruments was the TSI CPC model 3010 (TSI Inc., St. Paul, MN, USA;Sem 2002). The performance of this instrument has been thoroughly investigated both theoretically (Ahn and Liu 1990a) and experimentally (Ahn and Liu 1990b; Mertes et al. 1995; Ankilov et al. 2002; Wiedensohler et al. 1997; Hermann et al. 2007). The CPC 3010 was replaced in 2006 by the TSI models 3772 (TSI Inc., St. Paul, MN, USA; Hermann et al. 2007) and its modification for engine exhaust compliance measurements the CPC 3790 (TSI Inc., St. Paul, MN, USA; Giechaskiel et al. 2009). Both, the model 3772 and 3790 CPCs are laminar continuous flow type and butanol-based CPCs. The nominal flow rate is 1 L $min^{-1}$ and no sheath flow is used.

The CPC model 3790 is basically a detuned version of the 3772 with a reduced temperature difference between saturator and condenser, intended to shift the 50% cutoff diameter ($Dp_{50}$) from the nominal 10 nm of the CPC 3772 to 23 nm for the 3790, meeting the requirements of the UN-ECE regulation 83 for light duty vehicle nonvolatile particle number emissions.

Because this CPC type is one of the few commercially available instruments certified for engine exhaust compliance testing, its performance has been widely investigated. Several authors found a strong dependence on the chemical composition of the calibration material used for the 50% cutoff diameter determination (Wang et al. 2010; Mamakos et al. 2013). Furthermore, a degradation of the performance of the CPCs after extended use was noticed (Giechaskiel et al. 2011).

In this investigation, we summarize calibration results of 24 3772 CPCs and 9 3790 CPCs. These CPCs have been calibrated at the World Calibration Centre Aerosol Physics (WCCAP), hosted by the Leibniz Institute for Tropospheric Research (TROPOS), both in the context of routine measurements and within the ENV02 "Emerging requirements for measuring pollutants from automotive

**CONTACT** Thomas Tuch tuch@tropos.de Experimental Aerosol and Cloud Microphysics, Leibniz Institute for Tropospheric Research, Permoserstr. 15, Leipzig 04138, Germany.

Color versions of one or more of the figures in the article can be found online at www.tandfonline.com/uast.

exhaust emissions" project of the European Metrology Research Programme (EMRP). One new aspect obtained from these measurements is that the 50% cutoff mobility diameter does not only depend on particle chemical composition but—for the same chemical composition—also on particle morphology.

## Experimental setup

Particle generation: A silver condensation particle generator is used to generate monodisperse particles for CPC calibration at TROPOS. The generator is based on the design by Scheibel and Porstendörfer (1983). We have used a tube furnace with 3 separately temperature controlled heating zones (Linn model FRH-3-70/750/1250, Linn HighTherm GmbH, Eschenfelden, Germany) for particle generation. The heated length of this oven is 750 mm. During the experiments described here all three temperature zones have been set to the same temperatures. The sample material for evaporation is located in a boat in the center of a ceramic tube with an inner diameter of 19 mm.

The TROPOS silver aerosol generator (Figure 1) features an additional quench flow for faster cooling of the newly formed particles. In addition, the quench flow dilutes the aerosol from the oven to minimize coagulation of primary particles after generation. Both oven flow and quench flow are controlled by mass flow controllers (MKS model 1179AX14CS1BV; MKS Instruments Deutschland GmbH, Munich, Germany) to ensure better stability of the size distribution of the silver particles and better repeatability of calibration settings. A dilution system allows for concentration adjustment.

After dilution, the particles are sintered at 450°C to improve sphericity of the particles. The residence time in the first sintering oven is approximately 0.3 s. A cooling spiral of 1-m lenght is used to cool the aerosol down to room temperature.

The freshly generated polydisperse aerosol is neutralized by a custom made 370 MBq $^{85}$Kr neutralizer and fed into the TROPOS custom-made Hauke-type DMA (Winklmayr et al. 1991) at an aerosol flow of 1 l/min and a sheath air flow of 20 l/min for particle size selection (Figure 2).

During selection of monomobile particles the high voltage of the DMA is continuously adjusted to the temperature and pressure in the DMA by a custom-made LabView program to ensure repeatable particle size selections under varying ambient conditions. Alternatively, the same size selecting DMA can be operated in SMPS mode to determine the raw oven particle number size distribution. This option ensures that particles are selected from the right flank of the oven size distribution to reduce the number of multiple charge particles. After particle size selection, a turbulent diluter is used to add sufficient filtered air allowing for parallel calibration of up to seven candidate CPCs.

The candidate CPCs are connected to the common aerosol source using pipework designed to minimize differences between the ports, taking into account different diffusive losses due to the different flow rates of the CPCs by adjusting the length of the conductive tubing to each CPC, according to theoretical calculations. A length of 70 cm is used for the 1 l/min instruments, and aerocalc software (Willeke and Baron 2005) used to determine equivalent loss lengths for the other instruments.

An additional WCCAP reference mobility particle size spectrometer (Wiedensohler et al. 2012) monitors the particle number size distributions fed to the candidate CPCs. This mobility particle size spectrometer operates at 1 l/min aerosol flow and 5 l/min sheath air flow without a neutralizer in order to determine the fraction of multiple charged particles at larger particle sizes for electrometer correction. Sizing of this SMPS is verified with 203 nm PSL particles.

Both size selecting DMA and number size distribution measuring WCCAP reference SMPS use ISO 15900 (ISO 15900 2014) standards for diameter calculations. An example of typical number size distributions fed to the CPCs as measured by the reference SMPS is shown in Figure 3.

Three reference instruments are typically used for concentration measurements in this calibration setup. The main reference instrument is an aerosol electrometer (TSI model 3068B, TSI, St. Paul, MN, USA). This instrument has been calibrated by the National Metrology Institute of Germany (PTB) using a traceable fA source. Furthermore, the performance of this electrometer has been verified in an international intercomparison workshop of national metrological institutes (Hogström et al. 2014).

Because aerosol electrometers tend to be noisy at low particle number concentrations, two individually calibrated CPCs (TSI 3772 and 3025A) are added to

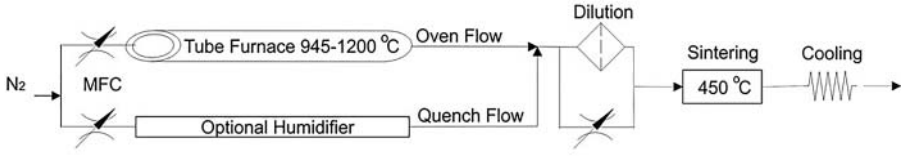


**Figure 1.** Schematic view of the TROPOS Ag aerosol generator.

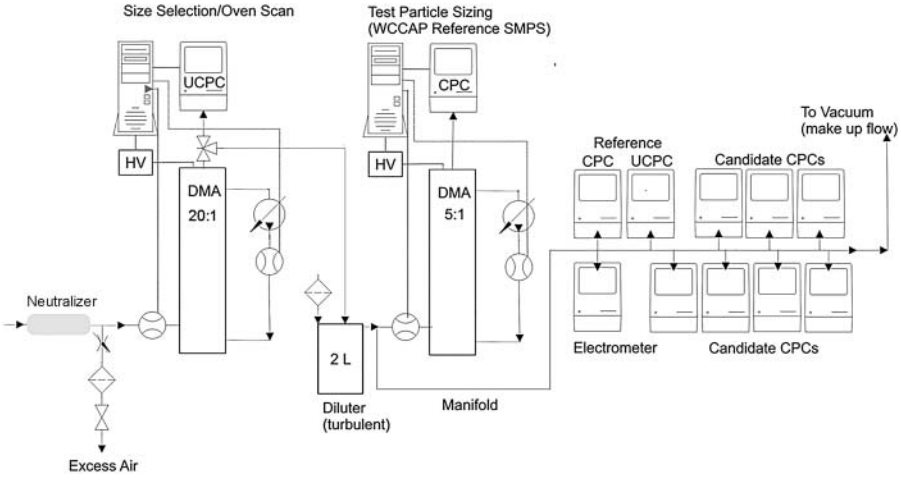


**Figure 2.** Size selection setup and calibration setup.

the setup. These CPCs are used as references at low concentrations. At the beginning and the end of each calibration run, number concentrations of 40 nm particles indicated by the CPC and UCPC are compared to those measured by the electrometer. While (multiple charge corrected) concentrations measured by the CPC must agree with the electrometer at this particle size number concentrations measured by the UCPC typically differ from the other instruments because of small deviations of the sample flow of the UCPC from its nominal value. This procedure determines the flow deviation of the UCPC from its standard value. Knowing the "real" sample flow the UCPC allows to use it as a reference for particle diameters smaller than 10 nm. Typically UCPC flows deviate by less than 10% from nominal values. If flow deviations exceed this 10% range specified by the manufacturer the UCPC cannot be used for calibration and needs both service and individual calibration prior to further usage.

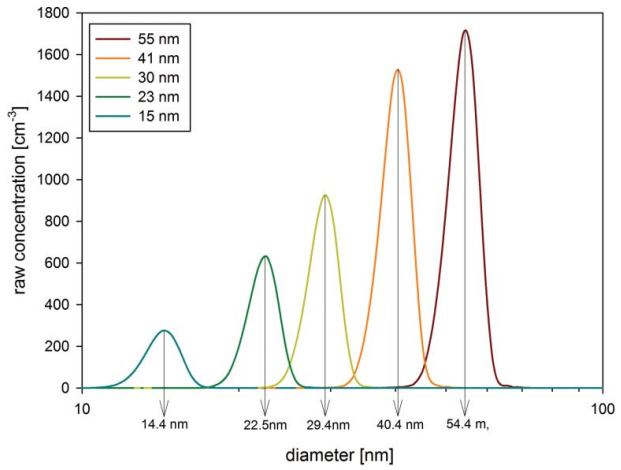


**Figure 3.** Typical number size distributions fed to the candidate CPCs measured by the reference SMPS.

Data acquisition in our setup is done by a custom LabView program counting pulses from the CPCs and calculating concentrations from the actual flow rates measured by a bubble flowmeter and count time. We typically use aerosol number concentrations of about 3000 $cm^{-3}$ minimizing coincidence effects at concentrations suitable for the aerosol electrometer.

In addition to the determination of the cut-off diameter at nominal and changed temperature differences between saturator and condenser we investigated the thermal stability of our calibration aerosol. For this purpose we used a secondary sintering over after size selection and dilution of the aerosol operated at 350°C in our calibration setup (Figure 4).

## Results and discussion

### *Counting efficiencies of TSI 3772 and 3790 CPCs*

Measurement of the particle size-dependent counting efficiencies curves of CPCs is routine at the WCCAP using the above experimental setup. The detection efficiency curve of twenty-four CPC model TSI-3772 is shown in the boxplot Figure 5.

The boxes in Figure 5 and 6 cover the 10th to 90th percentile of the data with a line in the box representing the average counting efficiency values of all CPCs for this diameter. Whiskers denominate outliers.

The average 50% detection efficiency diameter ± standard deviation, $Dp_{50}$, of model 3722 CPCs was found to be 7.52 ± 0.4 nm with a minimum of 6.37 nm and a maximum of 8.54 nm. The unit to unit variability described by average and standard deviation is in the same order of magnitude as found for a repeated calibration of one single (WCCAP reference) CPC over a time period of 1 year. For this repeated calibrations of this

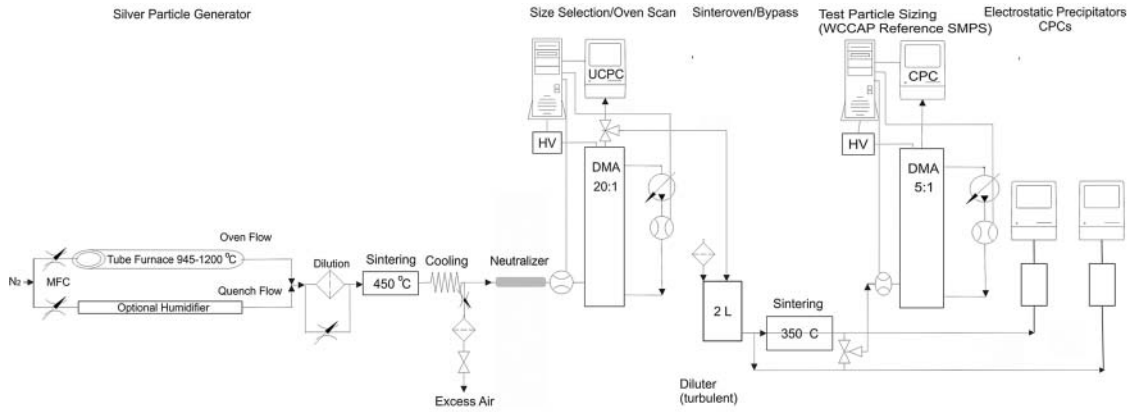


**Figure 4.** Calibration setup for thermal stability measurements.

CPC (~30) we found a 3 Σ range +− 0.5 nm with an average $D_{p50}$ of 7.8 nm.

All CPCs detected smaller particles than stated by manufacturer specifications (compared to the nominal $Dp_{50}$ of 10 nm when calibrated with sucrose particles as stated in the instrument manual). The regression curve shown in this plot can be parameterized according to ISO 27891 (Formula (1)).

$$Eff = 0.99 * \left[1 - exp\left(-\frac{(Dp - 5.46)}{(7.52 - 5.46)} * ln2\right)\right]$$

with

$$Eff = E_\infty * \left[1 - \exp\left(-\frac{(Dp - D_{p0})}{(D_{p50} - D_{p0})} * ln2\right)\right] \quad [1]$$

**Formula 1**. Regression curve for counting efficiencies of 3772 CPCs.

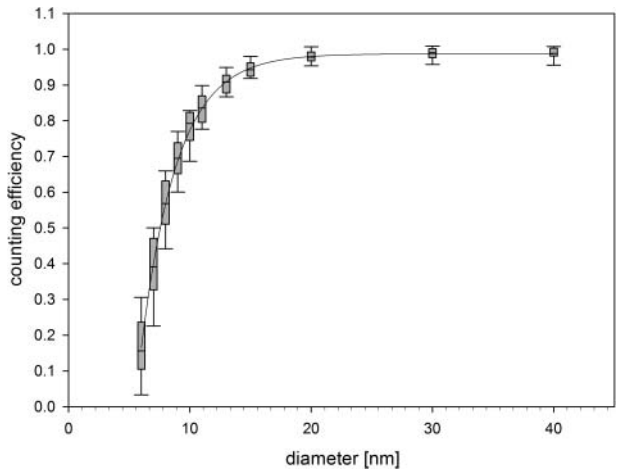


**Figure 5.** Boxplot and regression curve of detection efficiencies curve of 24 CPCs model TSI 3772.

$E_\infty$: Counting efficiency in the plateau region of the efficiency curve,

*Dp*: particle diameter, $D_{p50}$: 50% counting efficiency, and $D_{p0}$: Zero counting efficiency

Figure 6 shows the respective detection efficiency curve for the model 3790 CPCs with an average 50% detection efficiency diameter of 24.34 ± 0.29 nm. The minimum $Dp_{50}$ was found at 23 nm and the maximum 26 nm. Thus, all CPCs under investigation were within required specifications for engine exhaust compliance measurements. The regression formula for the counting efficiency curve is given in formula 2.

$$Eff = 1.02 * \left[1 - \exp\left(-\frac{(Dp - 16.71)}{(24.34 - 16.71)} * ln2\right)\right] \quad [2]$$

**Formula 2**. Regression curve for counting efficiencies of 3790 CPCs.

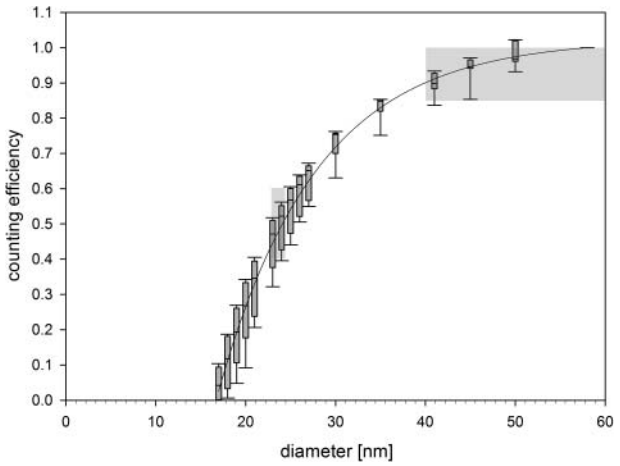


**Figure 6.** Boxplot and regression of particle detection efficiency curve of 9 CPCs model TSI 3790. The shaded rectangles denominate the tolerance limits for $Dp_{50}$ and $Dp_{90}$ required by UN-ECE regulation 83 for engine exhaust CPCs.

In both counting efficiency curves the plateau is not 1 because these regression curves have been calculated using original data with known uncertainties of the electrometer concentrations of +/−2% for 40 nm particles (Högström et al. 2014).

Both Formulas (1) and (2) describe the average performance of real 3772/3790 CPCs and may thereby yield a reference for the calibration of an individual instrument. Typical deviations from these curves are represented by the statistical information in Figures 5 and 6.

Our measurements of these recently calibrated (but not new) and new CPCs are in good agreement with findings previously reported in literature (Giechaskiel and Bergmann 2011). As reported in this article, new and recalibrated CPCs perform comparable when they are calibrated with the same type of aerosol. The CPCs investigated in our study have either been new (provided by the manufacturer) or used as reference instruments and calibrated prior to our experiments in both national metrological institutes or by engine manufacturers. They have (according to information provided by the owners) not been used for engine exhaust measurements.

## Effect of temperature difference between saturator and condenser on the cut-off diameter

Because 3790 CPCs are basically model 3772 CPCs with modified temperature difference between saturator and condenser in order to comply with engine exhaust measurement regulations, we investigated the influence of this temperature difference on the 50% counting efficiency diameter using two 3772 and one 3790 CPCs with modified condenser temperature at constant factory saturator temperature. The temperature difference dependencies of the 50% detection efficiency diameter are plotted in Figure 7. The equation for the regression line in this plot is given in Formula (3).

$$D_{p50} = 0.949 * \{exp(63.657/(\Delta T[K] + 11.577))\} \quad [3]$$

**Formula 3**. Regression formula for the influence of temperature difference $\Delta T$ between saturator and condenser in 3772 and 3790 CPCs on the cut-off diameter.

Typical condenser temperatures set during manufacturer maintenance of the 3790 CPCs ranged from 31.5°C to 31.7°C with saturator temperatures of 38.3°C resulting in temperature differences of 6.7 ± 0.1 K. These temperature difference settings for engine exhaust CPCs 3790 are in the steep slope of the temperature dependency curve. A change of temperature difference between saturator and condenser of +/−1 K will cause a shift of the 50% detection efficiency diameter from 24.34 to 20.6 nm and 26.4 nm (−18%,+8%), respectively. Our findings underline the necessity of tight temperature control of both saturator and condenser temperature in these engine exhaust CPCs.

Stability of the typical temperature difference in 3772 CPCs (17 K) is less critical at saturator temperatures of 39.0°C and 22.0°C condenser temperature with respect to a shift of the 50% detection efficiency diameter. In these instruments, a change of the temperature difference by +/−1 K would only cause a shift of the 50% detection efficiency diameter from 7.52 to 7.0 and 8.1 nm, respectively. Note that one CPC 3772 could be adjusted to a temperature difference between saturator and condenser of 27 K without homogenous nucleation of butanol vapor in the absence of aerosol particles. One second concentration measurements at this extreme setting showed a higher variability compared to CPCs operated at factory default temperature settings on the other hand these extreme setting shifted the 50% detection efficiency diameter down to 4 nm.

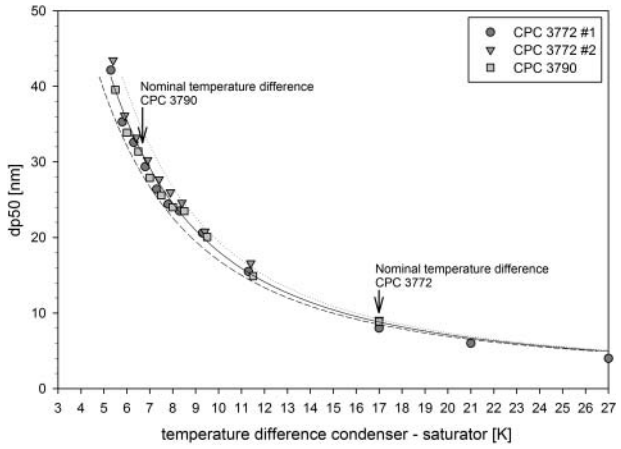


**Figure 7.** Dependence of the $Dp_{50}$ detection efficiency diameter on the temperature difference between saturator and condenser of two TSI CPCs 3772 and one TSI CPC 3790. The straight line represents the fit from formula 3, dashed lines represent the repeatability of $D_{p50}$ measurements with a single CPC within one year of operation (three standard deviations).

## Dependence of cut-off diameter on particle morphology

According to Scheibel and Porstendörfer (1983) silver particles generated by nucleation type aerosol generators with diameters smaller than 20 nm are spherical whereas larger particles are in the form of agglomerates. The TROPOS aerosol generator uses a sintering oven operated at 450°C directly after aerosol generation and dilution to improve sphericity of the particles (Figure 1).

We determined the number-size distribution of the silver particles after thermal treatment in a secondary

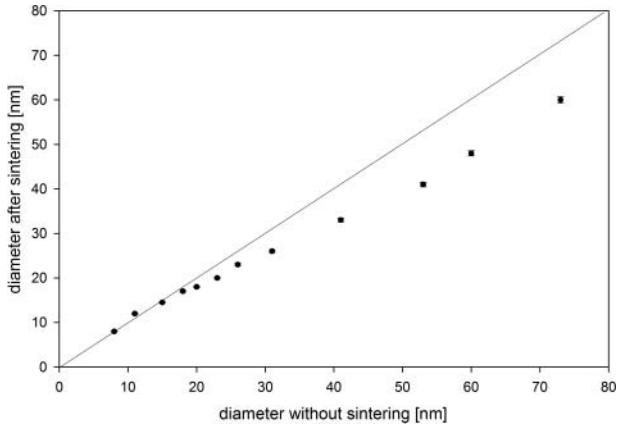


**Figure 8.** Mobility diameter of silver particles with and without secondary sintering after size selection by a DMA.

sintering oven using the WCCAP reference mobility particle size spectrometer of the setup. We observed that particles larger than 18 nm in our calibration setup shrink during the secondary sintering process as shown in Figure 8.

These results suggest that particles larger than 18 nm from this type of nucleation aerosol generator are not spherical even with sintering after the generating oven.

Transmission electron micrographs of untreated and secondary sintered 50 nm aerosol particles shown in Figure 9 reveal that particles without secondary sintering contain agglomerates, whereas particles are almost spherical with secondary sintering. Because only a minimal amount of silver evaporates at 350°C the observed shrinking of the particles can only be due to the change of particle morphology. A third sintering oven installed after the first to ovens did not cause further shrinking of the aerosol particles, suggesting that the particles in this setup have reached their final shape after the secondary sintering oven.

One possible reason for incomplete sintering in the first sintering oven could be the high initial concentration of the oven generated particles (about $10^6$ $cm^{-3}$) which can cause incomplete heat transfer to all particles in the oven. The particle number concentration of the size-selected aerosol is on the other hand significantly lower ($\sim 3 \times 10^3$ $cm^{-3}$) obviously allowing for complete sintering of the particles.

To investigate the influence of particle morphology on the particle detection efficiency curve of 3772 and 3790 CPCs, we determined 50% detection efficiency diameters with and without thermal treatment. Particle sizes were measured by the reference mobility particle size spectrometer and the size selecting DMA was adjusted to produce identical particles sizes both with and without sintering.

The detection efficiency curves for 3772 CPCs (squares) and 3790 engine exhaust CPC (triangles) with and without secondary sintering are presented in Figure 10.

This figure demonstrates that the detection efficiency curves of 3772 CPCs are virtually unaffected by the secondary sintering of the aerosol. This is due to the fact that the 50% detection efficiency diameters of these CPCs are smaller than 18 nm, where the particles generated in our setup were already spherical. On the other hand, the $Dp_{50}$ of 3790 engine exhaust CPCs was shifted from 25 nm to 28 nm. With identical chemical composition of the aerosol, this shift can be attributed to the different morphology of sintered and unsintered monomobile silver particles.

A theoretical explanation for the observed shift has been suggested (Kütz and Schmidt-Ott 1992; Crouzet and Marlow 1995). Particles in a CPC can only be detected if the size of the droplets formed by condensation on the particles exceeds the minimal detection limit of the optical particle counter used in the instrument. According to these papers, initial activation of aerosol particles depends on the contact angle θ between the particle and the condensed liquid. A contact angle of 0

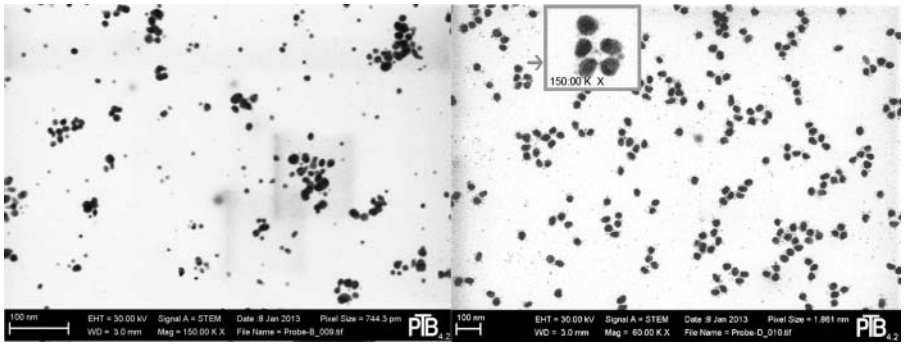


**Figure 9.** Change of silver particle morphology with sintering: TEM no sintering left, sintered right, 50 nm. Note the different magnification of the electron micrographs. Particles in the gray square of the right panel have been enlarged to match the magnification of the left panel.

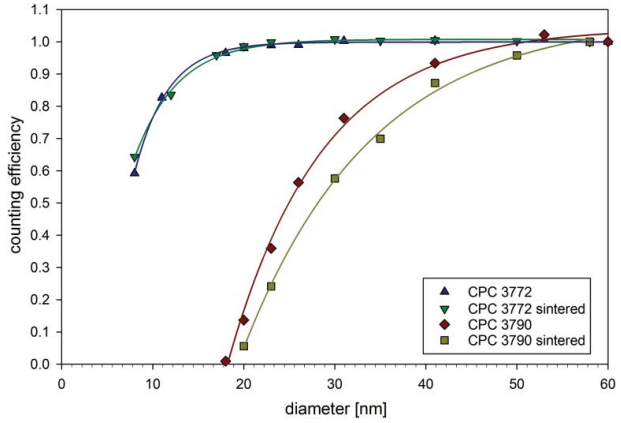


**Figure 10.** Average particle detection efficiency curves of 3772 and 3790 CPCs with and without secondary sintering of nucleation generated silver aerosol after size selection.



denominates complete wetting of the surface of the particle whereas 180 is associated with no wetting of the surface of the particle. Capillary condensation of butanol on the clusters grows particles with $\theta < 90$. The initial condensed mass per time, and thereby activation probability, is larger for smaller contact angles. Surfaces that are more spherical have larger contact angles than agglomerates. With identical thermal conditions and residence times in a CPC agglomerates have a higher probability for activation than more spherical particles. Once activated, all droplets will grow at identical growth rates to sizes detectable by the optical particle counter. The reduced activation probability of spherical particles compared to agglomerates thereby causes a shift of the cut-off diameters towards larger particles.

Our findings are relevant for measurements of particle number concentrations in engine exhaust. It is currently assumed (Burtscher 2005) that thermal treatment of exhaust gases is of no importance for the measurement of particle number concentration or EC mass, but it changes the size, surface, effective density, and fractal dimension of the soot particles. Changes in fractal dimensions of soot particles are typically attributed to condensation of volatile and semivolatile chemical compounds on the particle surface during dilution and thermal conditioning. With the absence of such compounds in our generator setup, our measurements suggest that the change of morphology during thermal treatment itself may affects particle number concentration measurements by shifting the $Dp_{50}$ of the CPCs.

## Conclusions

The performance of 24 model 3772 CPCs detected smaller silver particles than expected from manufacturer specifications, with an average 50% counting efficiency diameter of 7.5 nm. We could not observe effects of particle morphology on the 50% counting efficiency diameter for CPCs with $D_{p50}$ smaller than 15 nm because all particles smaller than 20 nm in diameter generated with the silver nucleation oven are already spherical. Our current setup without secondary sintering is, therefore, suitable for most standard CPCs. Small changes of the temperature difference between saturator and condenser temperatures in these CPC cause only small shifts of the 50% counting efficiencies. All 9 3790 CPCs performed within manufacturer specifications and within PMP conform legislation. The 50% counting efficiencies of these CPCs were, however, subject to significant shifts in particle size depending on the exact temperature difference between saturator and condenser, and on particle morphology. Our study presents initial evidence for the influence of particle morphology on CPC counting efficiencies. Further experiments like fractal analysis of the particles are needed to investigate the effects of particle morphology in detail.

## Funding

This work was supported by the German federal environmental agency FKZ 35101086 (WBA-WCCAP), ACTRIS and by the European Metrology Research Program (EMRP), jointly funded by the EMRP participating countries within EURAMET and the European Union.

## References

Agarwal, J. K., and Sem, G. J. (1980). Continuous Flow, Single-Particle-Counting Condensation Nucleus Counter. *J. Aerosol Sci.*, 11(4):343–357.

Ahn, K. H., and Liu, B. Y. (1990a). Particle Activation and Droplet Growth Processes in Condensation Nucleus Counter—I. Theoretical Background. *J. Aerosol Sci.*, 21 (2):249–261.

Ahn, K. H., and Liu, B. Y. (1990b). Particle Activation and Droplet Growth Processes in Condensation Nucleus Counter—II. Experimental Study. *J. Aerosol Sci.*, 21(2):263–275.

Ankilov, A., Baklanov, A., Colhoun, M., Enderle, K. H., Gras, J., Julanov, Y., and Zagaynov, V. (2002). Particle Size Dependent Response of Aerosol Counters. *Atmos. Res.*, 62 (3):209–237.

Bricard, J., Delattre, P., Madelaine, G., and Pourprix, M. (1976). *Fine Particles*, Liu, B. Y. H., ed., Academic Press, New York.

Burtscher, H. (2005). Physical Characterization of Particulate Emissions from Diesel Engines: A Review. *J. Aerosol Sci.*, 36 (7):896–932.

Crouzet, Y., and Marlow, W. H. (1995). Calculations of the Equilibrium Vapor Pressure of Water Over Adhering 50–200-nm Spheres. *Aerosol Sci. Technol.*, 22(1):43–59.

Giechaskiel, B., Wang, X., Horn, H. G., Spielvogel, J., Gerhart, C., Southgate, J., and Krasenbrink, A. (2009). Calibration of

Condensation Particle Counters for Legislated Vehicle Number Emission Measurements. *Aerosol Sci. Technol.*, 43 (12):1164–1173.

Giechaskiel, B., Wang, X., Gilliland, D., and Drossinos, Y. (2011). The Effect of Particle Chemical Composition on the Activation Probability in n-Butanol Condensation Particle Counters. *J. Aerosol Sci.*, 42(1):20–37.

Giechaskiel, B., and Bergmann, A. (2011). Validation of 14 Used, Re-Calibrated and New TSI 3790 Condensation Particle Counters According to the UN-ECE Regulation 83. *J. Aerosol Sci.*, 42(3):195–203.

Hermann, M., Wehner, B., Bischof, O., Han, H. S., Krinke, T., Liu, W., Zerrath, A., and Wiedensohler, A. (2007). Particle Counting Efficiencies of New TSI Condensation Particle Counters. *J. Aerosol Sci.*, 38(6):674–682.

Högström, R., Quincey, P., Sarantaridis, D., Lüönd, F., Nowak, A., Riccobono, F., Tuch, T., and Yli-Ojanperä, J. (2014). First comprehensive inter-comparison of aerosol electrometers for particle sizes up to 200 nm and Concentration Range 1000 $cm^{-3}$ to 17 000 $cm^{-3}$. *Metrologia*, 51(3):293.

ISO 15900 (2014). Determination of Particle Size Distribution—Differential Electrical Mobility Analysis for Aerosol Particles. http://www.iso.org/iso/catalogue_detail.htm?csnumber=39573.

Kütz, S., and Schmidt-Ott, A. (1992). Characterization of Agglomerates by Condensation-Induced Restructuring. *J. Aerosol Sci.*, 23:357–360.

Mamakos, A., Giechaskiel, B., and Drossinos, Y. (2013). Experimental and Theoretical Investigations of the Effect of the Calibration Aerosol Material on the Counting Efficiencies of TSI 3790 Condensation Particle Counters. *Aerosol Sci. Technol.*, 47(1):11–21.

Mertes, S., Schröder, F., and Wiedensohler, A. (1995). The Particle Detection Efficiency Curve of the TSI-3010 CPC as a Function of the Temperature Difference Between Saturator and Condenser. *Aerosol Sci. Technol.*, 23 (2):257–261.

Scheibel, H. G., and Porstendörfer, J. (1983). Generation of Monodisperse Ag- and NaCl Aerosols with Particle Diameters Between 2 and 300 nm. *J. Aerosol Sci.*, 2:113–126.

Sem, G. J. (2002). Design and Performance Characteristics of Three Continuous-Flow Condensation Particle Counters: A Summary. *Atmos. Res.*, 62(3):267–294.

Sinclair, D., and Hoopes, G. S. (1975). A Continuous Flow Condensation Nucleus Counter. *J. Aerosol Sci.*, 6(1):1–7.

UN ECE 83. http://www.unece.org/fileadmin/DAM/trans/main/wp29/wp29regs/r083r4e.pdf

Wang, X., Caldow, R., Sem, G. J., Hama, N., and Sakurai, H. (2010). Evaluation of a Condensation Particle Counter for Vehicle Emission Measurement: Experimental Procedure and Effects of Calibration Aerosol Material. *J. Aerosol Sci.*, 41(3):306–318.

Wiedensohler, A., Birmili, W., Nowak, A., Sonntag, A., Weinhold, K., Merkel, M., Wehner, B., Tuch, T., Pfeifer, S., Fiebig, M., Fjäraa, A. M., Asmi, E., Sellegri, K., Depuy, R., Venzac, H., Villani, P., Laj, P., Aalto, P., Ogren, J. A., Swietlicki, E., Williams, P., Roldin, P., Quincey, P., Hüglin, C., Fierz-Schmidhauser, R., Gysel, M., Weingartner, E., Riccobono, F., Santos, S., Grüning, C., Faloon, K., Beddows, D., Harrison, R., Monahan, C., Jennings, S. G., O'Dowd, C. D., Marinoni, A., Horn, H.-G., Keck, L., Jiang, J., Scheckman, J., McMurry, P. H., Deng, Z., Zhao, C. S., Moerman, M., Henzing, B., de Leeuw, G., Löschau, G., and Bastian, S. (2012). Mobility particle size spectrometers: harmonization of technical standards and data structure to facilitate high quality long-term observations of atmospheric particle number size distributions. *Atmospheric Measurement Techniques*, 5:657–685.

Wiedensohler, A., Orsini, D., Covert, D. S., Coffmann, D., Cantrell, W., Havlicek, M., …, and Litchy, M. (1997). Intercomparison Study of the Size-Dependent Counting Efficiency of 26 Condensation Particle Counters. *Aerosol Sci. Technol.*, 27(2):224–242.

Willeke, K., and Baron, P. (2005). *Aerosol Measurement: Principles, Techniques, and Applications*. Van Nostrand Reinhold, New York.

Winklmayr, W. G. P. A. O. A., Reischl, G. P., Lindner, A. O., and Berner, A. (1991). A New Electromobility Spectrometer for the Measurement of Aerosol Size Distributions in the Size Range from 1 to 1000 nm. *J. Aerosol Sci.*, 22(3):289–296.